

DISTRIBUTION OF HEAT DUE TO BEAM LOSS
IN ENERGY DOUBLER/SAVER TYPE SUPERCONDUCTING MAGNETS

A. Van Ginneken

September 13, 1976

Introduction

The problem of quenching of superconducting magnets due to heating induced by accidental beam bombardment has been raised ever since such magnets have been proposed in the design of accelerators, storage rings and beam transport lines. With the currently intense interest in building such facilities at Fermilab and elsewhere, some results of calculations pertaining to this problem are reported here.

An analysis of this problem divides naturally into two parts: (1) the spatial distribution of energy (heat) deposition in the magnet, and (2) the subsequent heat transport through the magnet (in the presence of cryogenic cooling). A recent study¹ of this subject has examined the energy deposited in a number of simple geometries along with a cursory treatment of heat transport. The present note concentrates on the energy deposition part of the analysis. An attempt is made to make the beam loss conditions somewhat more realistic. While some results of specific calculations are presented, the purpose of this is largely illustrative since these results tend to be quite sensitive to various parameters of the calculation.

The results shown here are obtained with the Monte Carlo program CASIM.² Comparisons of prediction of CASIM with results of recent Fermilab experiments^{3,4} have been quite satisfactory. The excellent agreement with a target heating experiment³ is of particular interest here.

Beam and Magnet Geometry

The magnet model geometry used in the analysis is based on a proposed (E series) Doubler/Saver bending magnet. Figure 1a is a sketch of the magnet and Figure 1b of the simplified model employed in the calculation. Note that the rather complicated geometry exhibited by the superconductor coils, supports and voids located between the cooling tubes has been represented by solid iron. This is actually a good approximation to a weighted average of the atomic number, mass and density of the materials present in that region. A beam momentum of 1000 GeV/c is assumed in all calculations. In the presence of a magnetic field the resulting energy deposition will obviously depend on the azimuthal location of the beam loss. The choice made here, shown in Figure 1b, is expected to result in the largest maximum energy deposition in the superconducting coils since the (positive) beam is deflected radially outward i.e. in the direction of the shortest distance to the coils.

Results of four specific calculations are reported here. The first two correspond to the case of beam being scraped off on the wall of a beampipe in an accelerator or storage ring. A

beam of infinitesimal lateral extent is introduced an infinitesimal distance into the wall travelling parallel to the magnet axis. This calculation has been performed with and without a magnetic field. In the former case the field components (maximum 42.3 kG) are described numerically on a 16x24 interpolation grid taken from a computation of the field, specifically for the magnet of Figure 1a, using the program LINDA.⁵ Correlated sampling has been used to minimize statistical differences between the calculation with and without magnetic field.⁶ The third calculation is typical for beam being lost in an external beam line. In the case of complete failure of a magnet the beam would enter the wall at an angle with the axis roughly equal to ℓ/r where ℓ is the length of the magnet and r the radius of curvature of the beam. At Fermilab this is typically 6 mrad. For this mode of beam loss the lateral extent and spatial distribution of the beam are very important. For the present calculation it has been assumed that the beam has a Gaussian profile with a standard deviation of 0.15 cm.

Finally a rough simulation of beam interaction with an internal target has been made. The geometry adopted is an infinitesimal interaction volume followed by a 20 m long evacuated drift space followed in turn by a 20 m long dipole. This calculation also was performed with and without magnetic field.

Results

For the purpose of estimating the spatial distribution of energy deposition the magnet is divided into volume bins. These are delineated by planes of constant Z (magnet axis), half-planes of constant azimuthal angle, ϕ , and cylindrical surfaces of constant radius, R . The length of the bins ΔZ ranges between 5 and 50 cm, $\Delta\phi$ varies from 0.01 to $\pi/4$ radians and ΔR is either 0.3 or 0.4 cm. For most of the results presented below the smaller volume bins are combined to improve statistical significance. Since reflection symmetry between bins of equal but opposite sign of ϕ obtains these bins have been combined.

The longitudinal variation of the energy deposition at small ϕ is shown in Figure 2(a-c) for each of the first three cases and for the inner and outer radial regions located between the cooling tubes. All plots show the typical transition curve. The longitudinal region $150 < Z < 200$ cm is seen, in each case, to be at or near the maximum of the curve. Note that for the case of magnet failure, the failed magnet does not necessarily intercept a large share of the energy deposited. Assuming the dimensions of Figure 1 and the length of the magnet to be 6 m, the maximum energy deposited in the coils typically occurs in the magnet following the failed one at about one meter from its upstream end. Figure 2c can then be used to determine if this magnet as well as its neighbor downstream is likely to fail.

The radial variation in the $150 < Z < 200$ cm range is plotted in Figure 3(a-c) for various azimuthal regions including a region near $\phi=0$ within which the calculation shows no significant variation with ϕ . This is a much smaller region for the case of the 6 mrad incident beam compared with the parallel beam. Also, as expected, the azimuthal dependence becomes much less pronounced at larger radii. (The reversal between the values for $0 < \phi < 0.01$ and $0.05 < \phi < 10.0$ with increasing R in Figure 3c is, of course, strictly of statistical origin.) By assuming an exponential behavior of the energy deposition with radius over the first two radial bins ($0 < R < 0.7$ cm) the maximum energy deposited may be estimated. These values are indicated in Figure 3.

Figure 4(a-c) presents the azimuthal variation for various radial regions and again for $150 < Z < 200$ cm. A radius of 1.50 cm corresponds roughly to the outer radius of the superconducting coils. For this reason the region $1.10 < R < 1.50$ cm shown in Figure 4 may be of interest.

The results of this study confirm the expectation that the energy density distribution is highly sensitive to a number of input parameters: geometry, beam size, magnetic field, etc. The variation in maximal energy deposition between the three cases which are shown in Figure 3(a-c), typifies this sensitivity. The introduction of the magnetic field results in an increase of

about a factor of three in the maximum energy density because of the deflection of the (positive) beam toward the coils. In addition to the beam particles the more energetic leading particles and to a lesser extent also the more energetic produced particles will tend to be positive. Medium energy protons ejected from nuclei will also be significantly influenced by the field. The case of an incident beam at 6 mrad ($\vec{B}=0$) yields an increase of about a factor of 70 compared with parallel incidence. A significant increase is expected since for the 6 mrad case the cascade axis intersects the coils after traversing a total of about two interaction lengths of material. However, a quantitative expression of this increase will depend strongly on a number of other input parameters as well.

Figure 5(a,b) shows the longitudinal dependence of the energy deposited in the innermost radial region of the coils for the simulation of the internal target problem, respectively with and without magnetic field. The difference is striking. The maximum energy deposition appears larger by a factor of about seven with the magnetic field present. As the azimuthal dependence (Figure 5a) shows, the effect of the field is to sweep charged particles entering the magnet within the beampipe into the coils. For reasons already mentioned the effect is largest for positive particles. The azimuthal angular region near $\phi \approx \pi$ also shows an increase (due to negative particles). In Figure 5a this is partially masked by the larger bin size.

Finally as an aid to the interpretation of Figures 2-5, equation (2) of Reference 1 which connects the adiabatic temperature increase measured from liquid He temperature (i.e. $T-4.2^{\circ}\text{K}$, where T is the final temperature) with energy deposition in the units employed here is presented in graphical form in Figure 6 over a useful range of temperature change. A more sophisticated analysis of this part of the problem, though no doubt necessary to arrive at valid conclusions about quenching, is not attempted at this time.

In addition to calculating density of energy deposition the program CASIM also computes density of nuclear interactions and momentum spectra of hadrons in selected regions of the magnets. These results may be useful for estimating e.g. radioactivation of the materials and radiation damage.

I am indebted to S. Snowdon for providing the detailed magnetic field map used in the calculation. I wish to thank M. Awschalom, D. Edwards, P. Gollon and P. Sanger for discussion. R. R. Wilson pointed out the internal target problem.

REFERENCES

- ¹C. Restat, H. Schönbacher and M. Van de Voorde, The Effect of Radiation Heating on Superconducting Coils, CERN ISR-MA/75-20 (1975).
- ²A. Van Ginneken and M. Awschalom, High Energy Particle Interactions in Large Targets. Vol. I - Hadronic Cascades, Shielding and Energy Deposition, Fermilab, Batavia, IL (1975);
A. Van Ginneken, CASIM. Program to Simulate Transport of Hadronic Cascades in Bulk Matter, Fermilab FN-272 (1975).
- ³M. Awschalom et al., Nucl. Inst. Meth. 31, 235 (1975).
- ⁴M. Awschalom et al., Measurements and Calculations of Cascades Produced by 300 GeV Protons Incident on a Target Inside a Magnet, Fermilab-PUB-76/48-EXP (1976).
- ⁵J. Colonias, Particle Accelerator Design: Computer Programs, Academic Press, New York, NY (1974).
- ⁶A. Van Ginneken, Effects of Magnetic Fields on Hadronic Cascades, Fermilab TM-657 (1976).

FIGURE CAPTIONS

- Fig. 1: (a) Sketch of proposed E series magnet for Energy Doubler/Saver. All measurements are in inches. (b) Idealization of this magnet used in Monte Carlo calculation. All measurements are in cm.
- Fig. 2: Longitudinal variation of energy deposition at small ϕ , for $0 < R < 0.3$ cm, the region of largest energy deposition in the superconductor, and for the region $2.3 < R < 2.7$ cm adjacent to the outer cryogenic cooling tube. (a) Zero degree incidence, no magnetic field, (b) with magnetic field, (c) 6 mrad incidence, no magnetic field, beam has Gaussian profile $\sigma = 0.15$ cm. R is measured from the inner radius of the superconducting coils. Z is measured from the point where the beam (or beam center) intercepts the beampipe. ϕ is measured from the y axis (Fig. 1b).
- Fig. 3: Radial variation of energy deposition for various regions of ϕ and/or $150 < Z < 250$ cm. (a), (b), and (c) as in Fig. 2. The point plotted at $R = 0$ is an estimate of the maximum energy density.
- Fig. 4: Azimuthal variation of energy deposition for various radial regions and for $150 < Z < 250$ cm. (a), (b), and (c) as in Fig. 2.
- Fig. 5: Longitudinal variation of energy deposition for the region ($0 < R < 0.3$ cm) adjacent to the inner cryogenic cooling tube of magnet 20 m downstream of an infinitesimally small interaction volume (a) with magnetic field (b) without magnetic field.
- Fig. 6: Adiabatic temperature increase of copper (starting at 4.2°K) versus energy density.¹

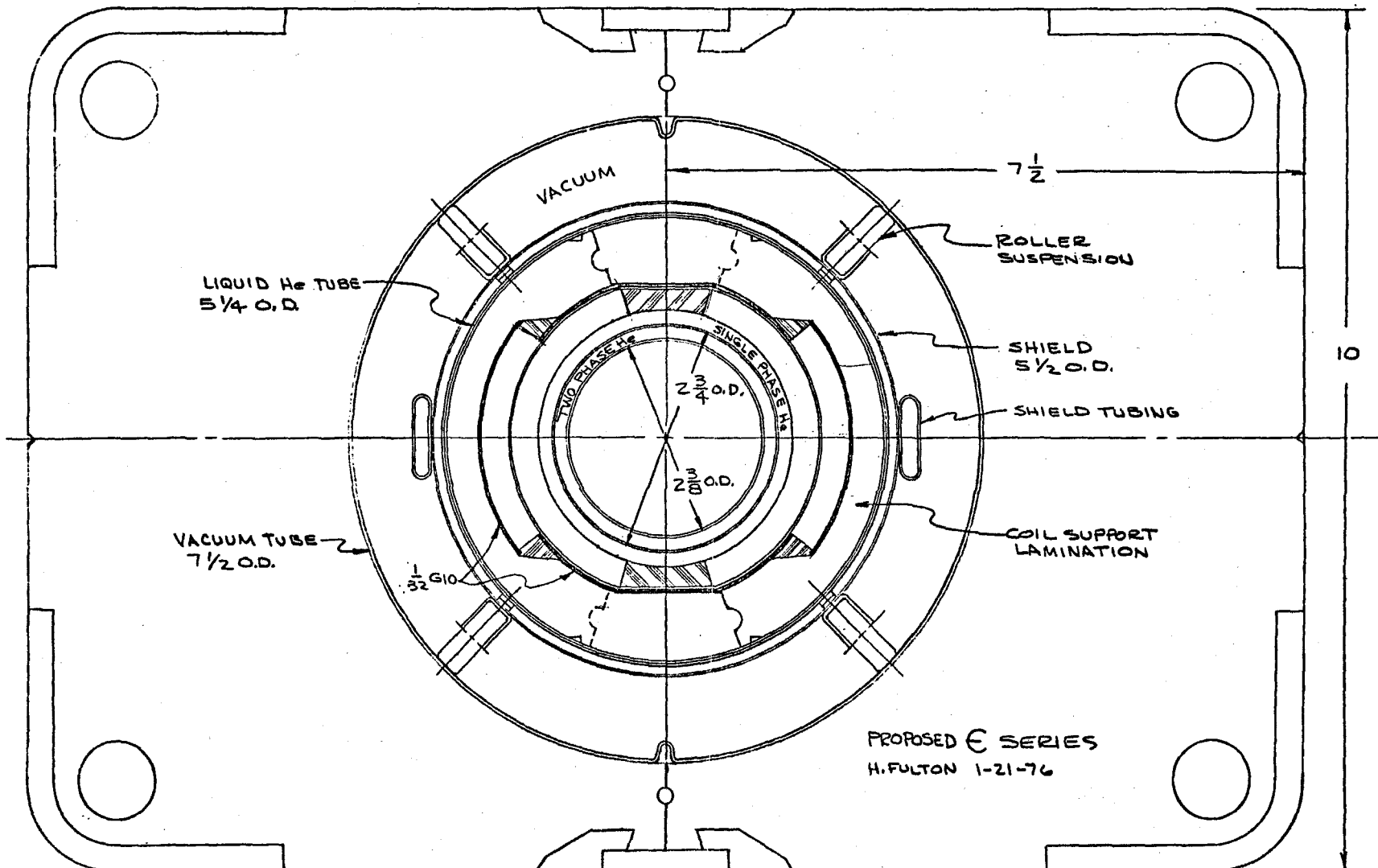


Fig. 1a

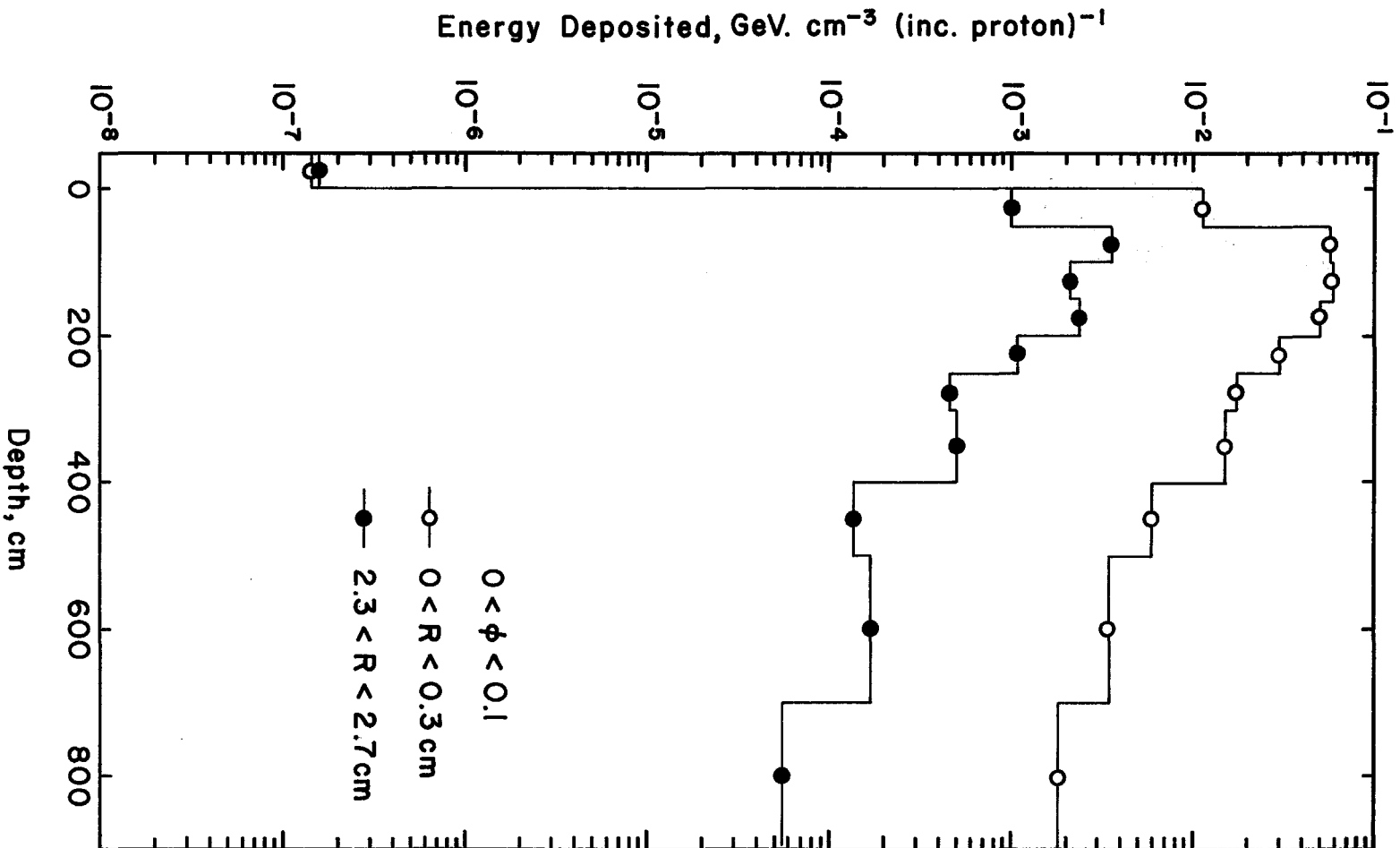


Fig. 2a

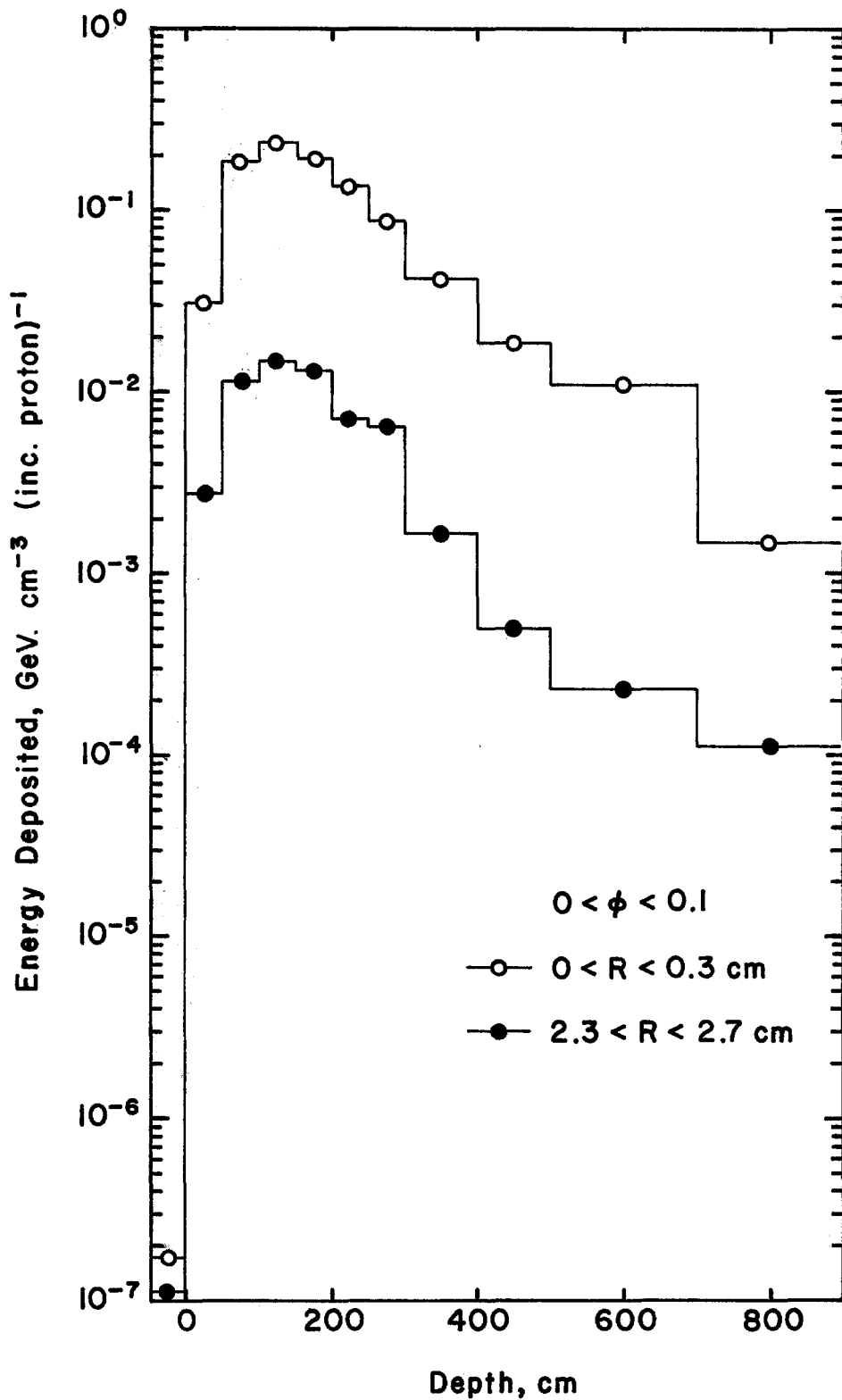


Fig. 2b

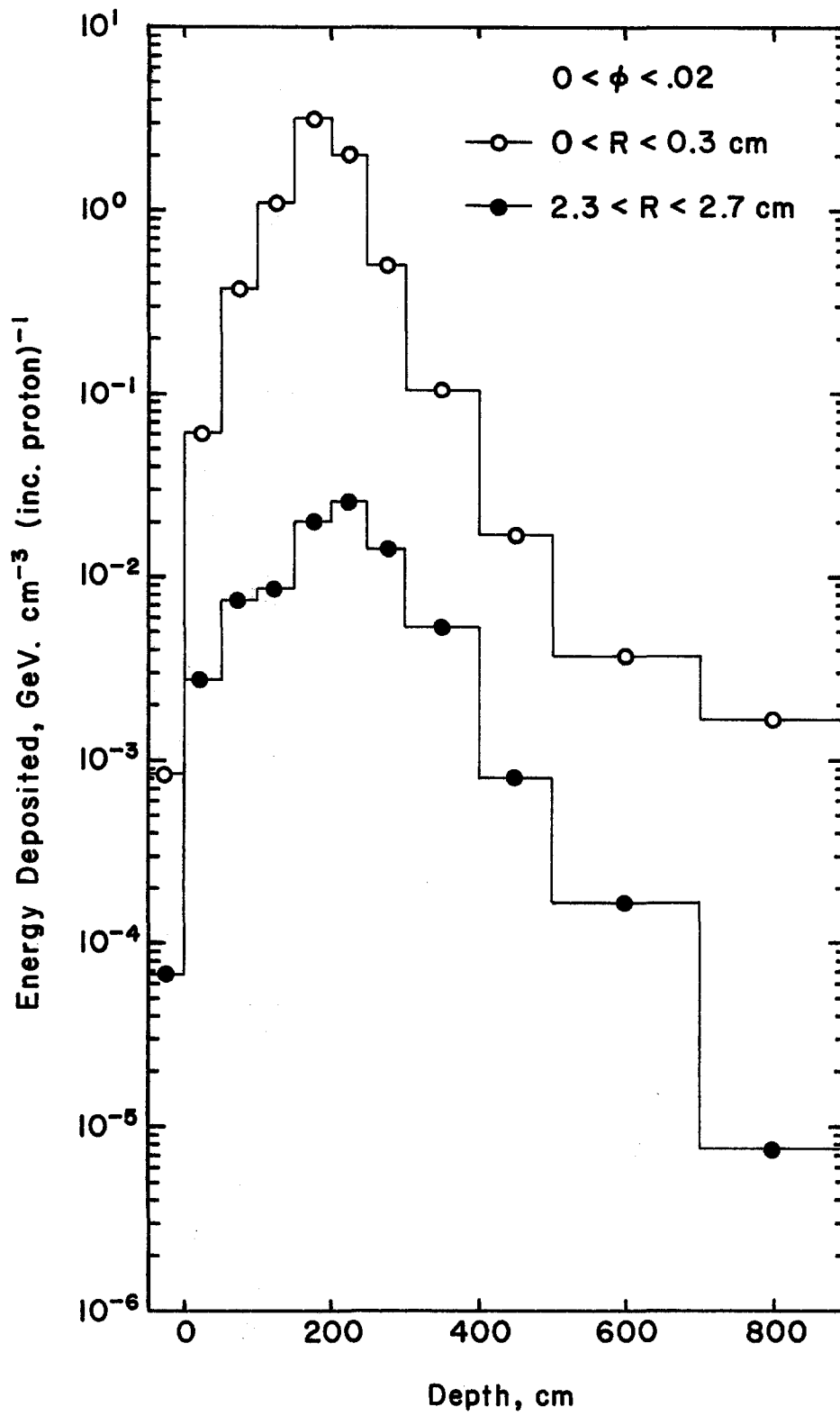


Fig. 2c

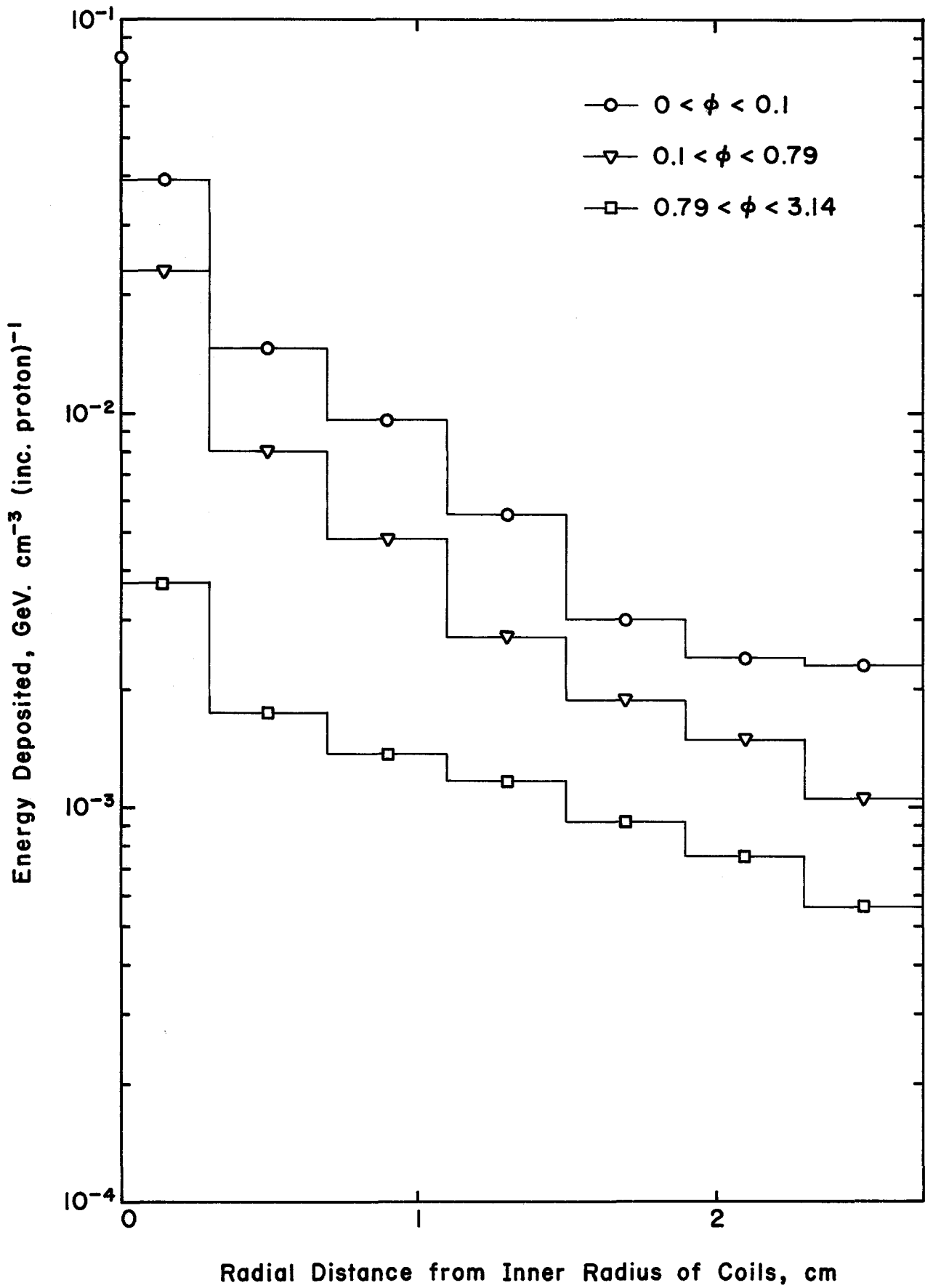


Fig. 3a

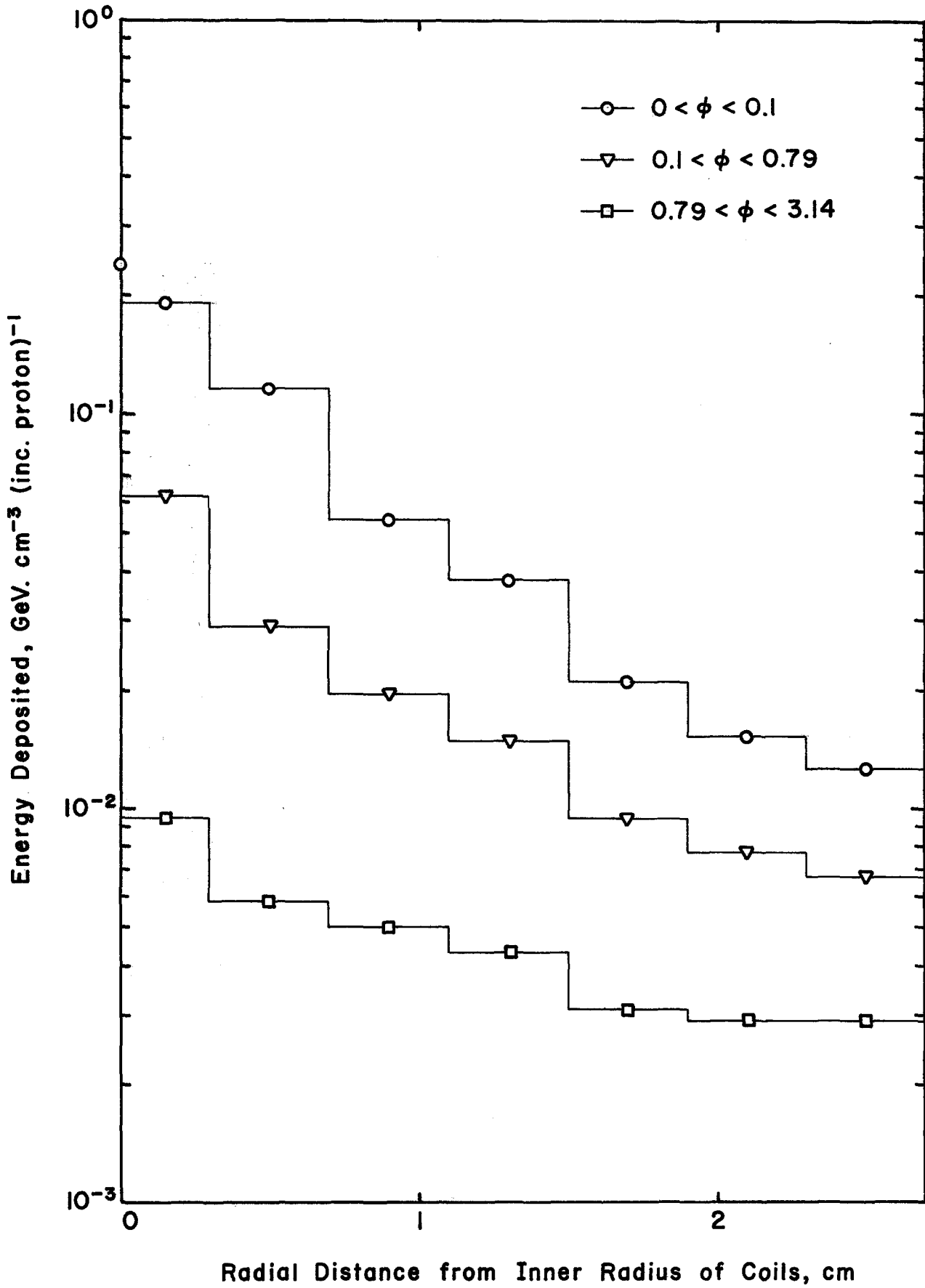


Fig. 3b

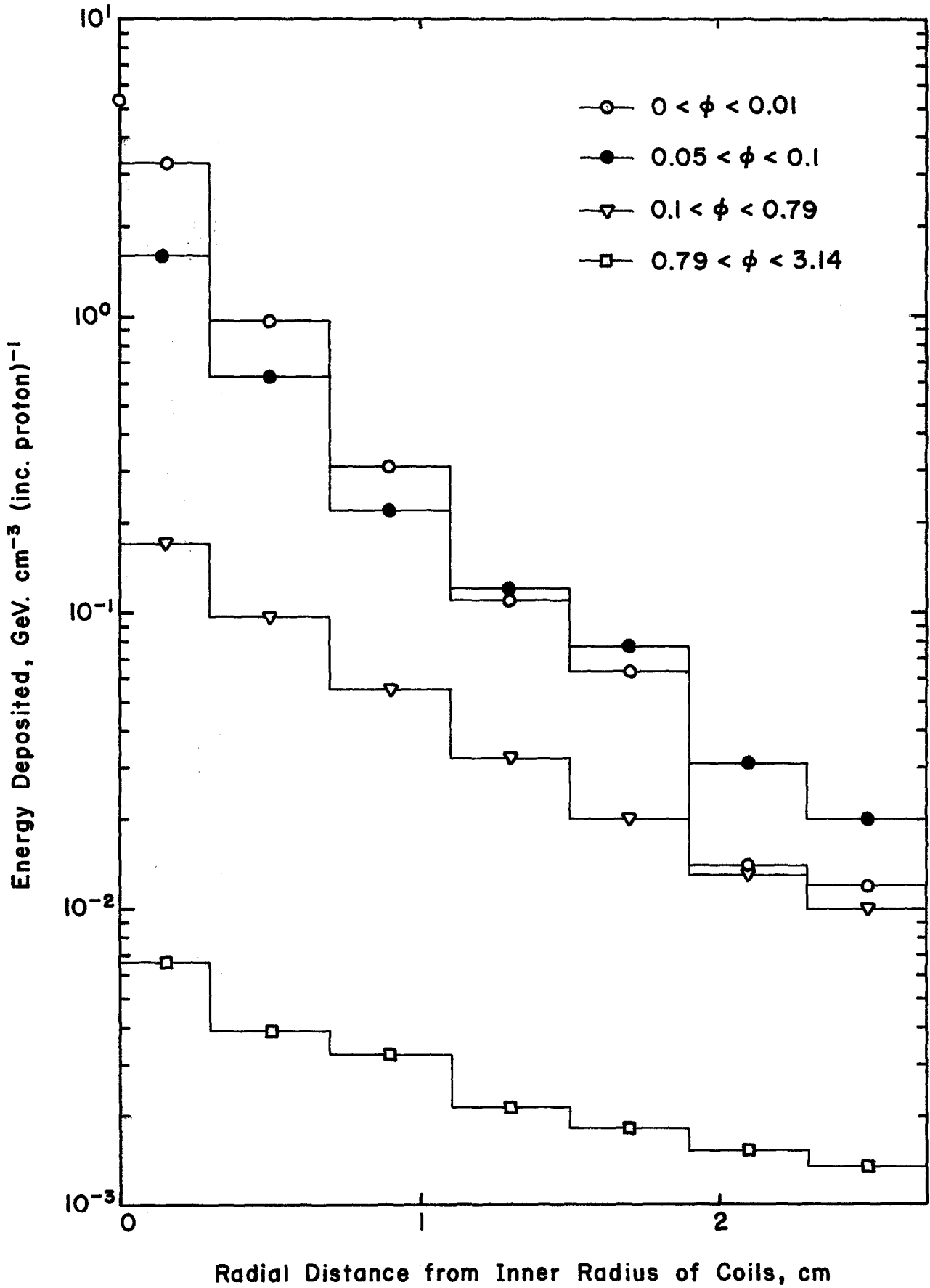


Fig. 3c

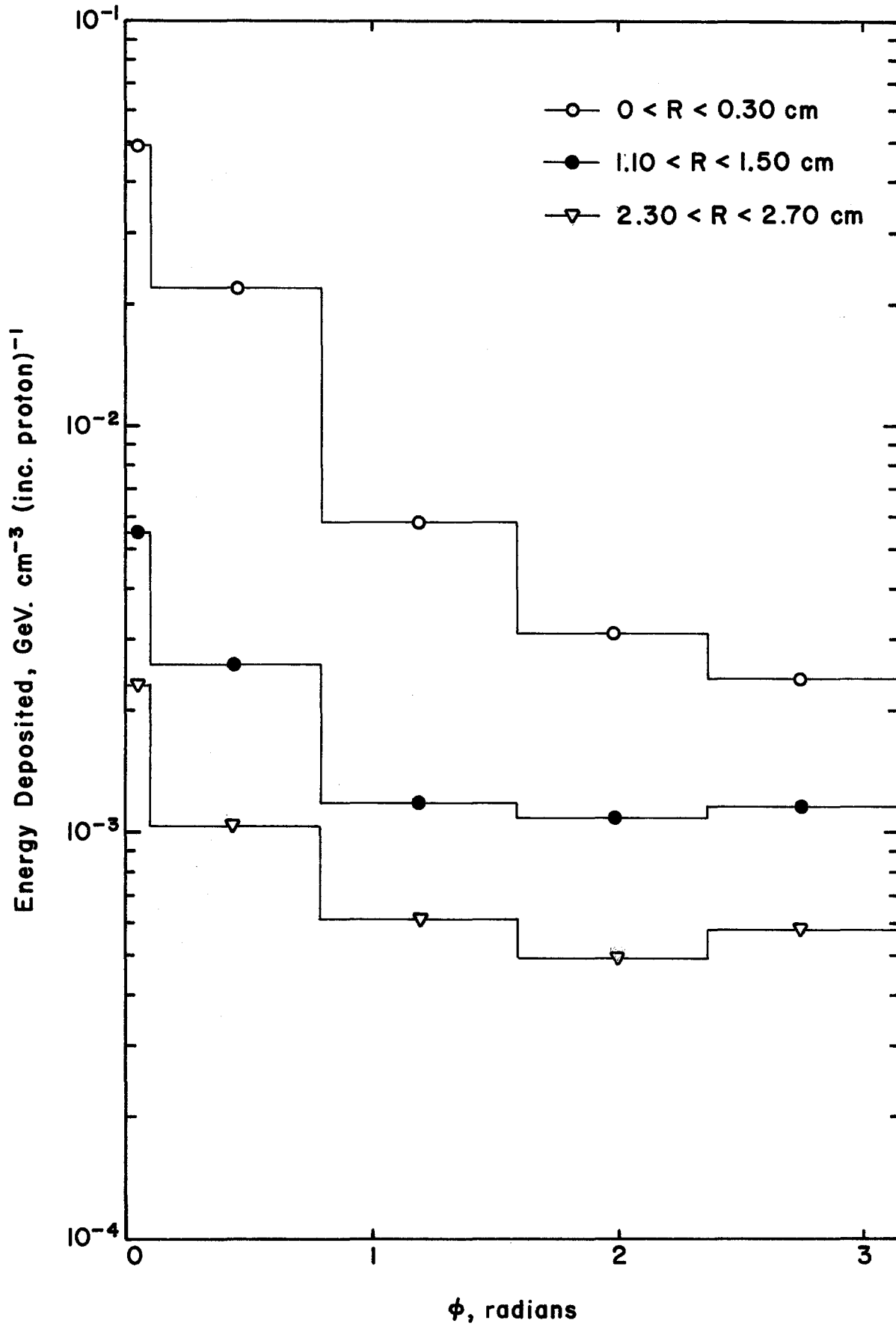


Fig. 4a

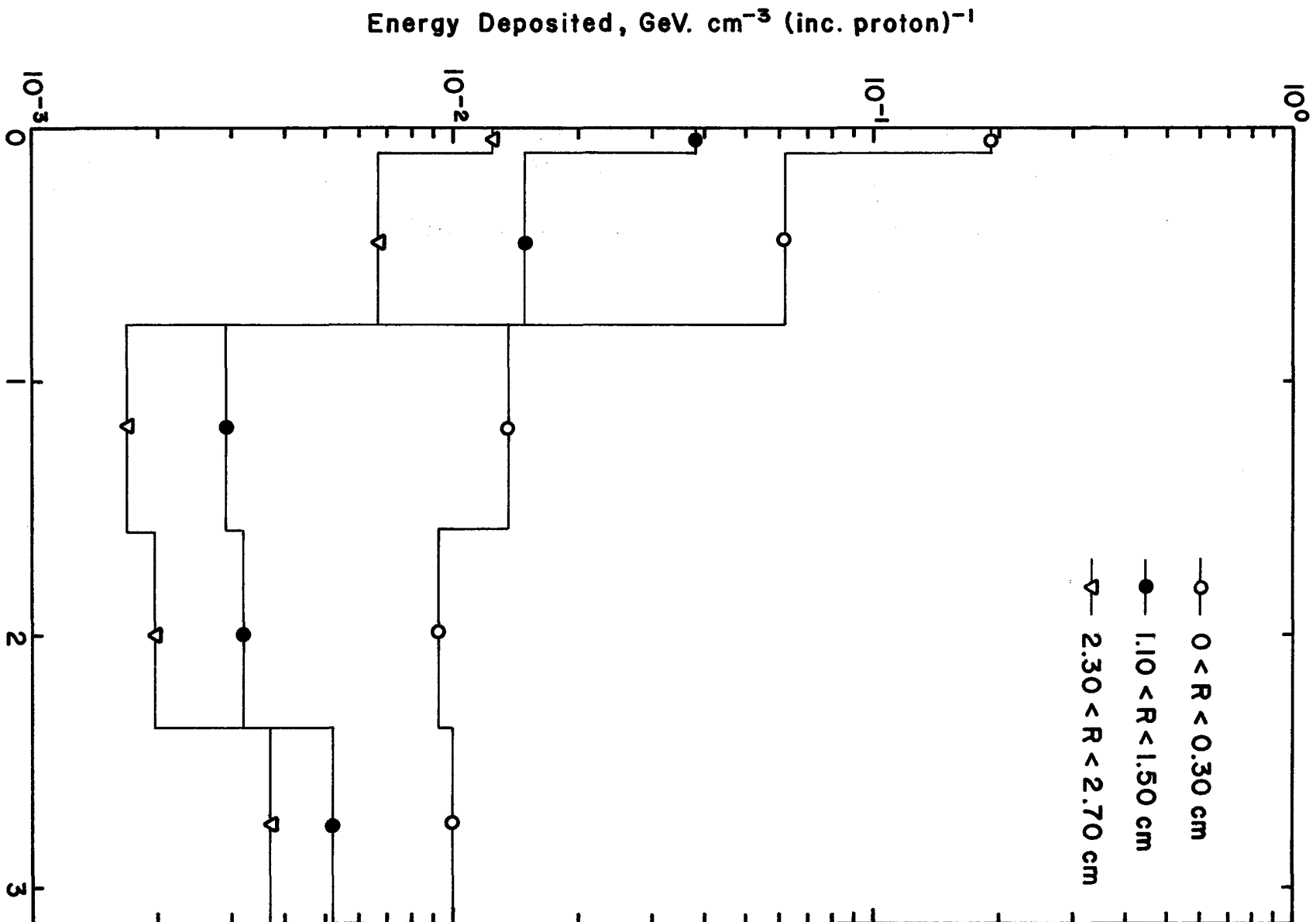


Fig. 4b

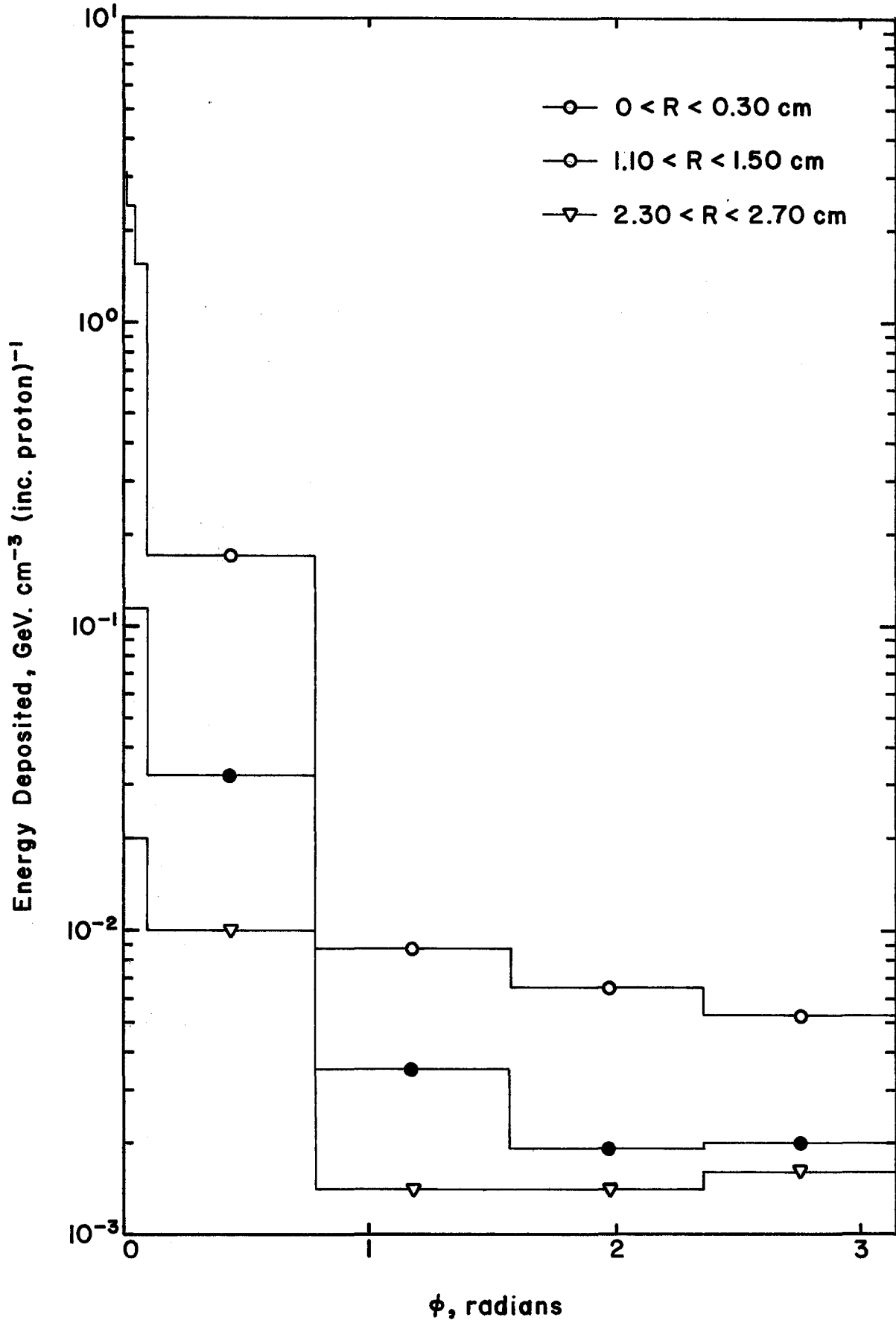


Fig. 4c

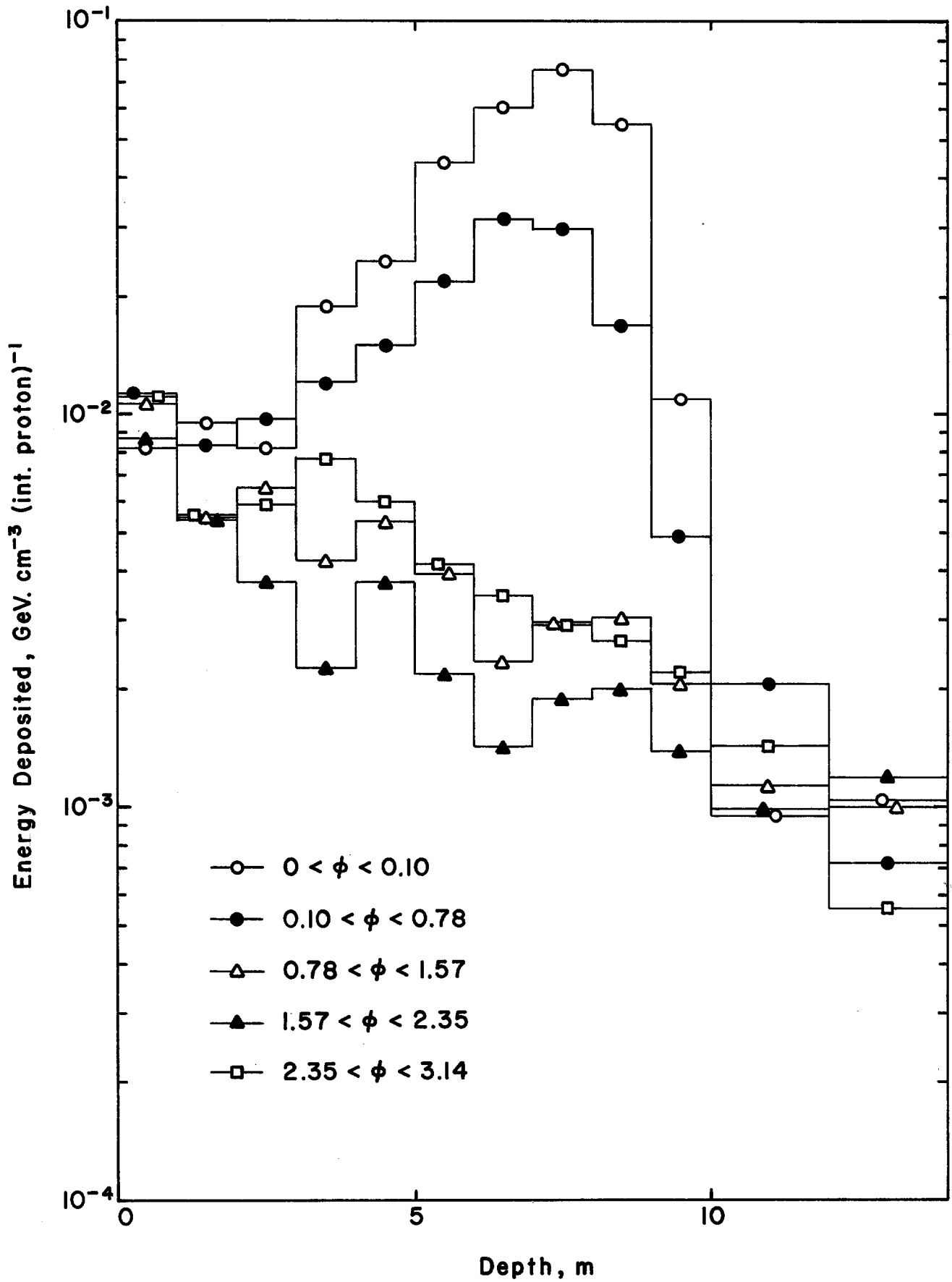


Fig. 5a

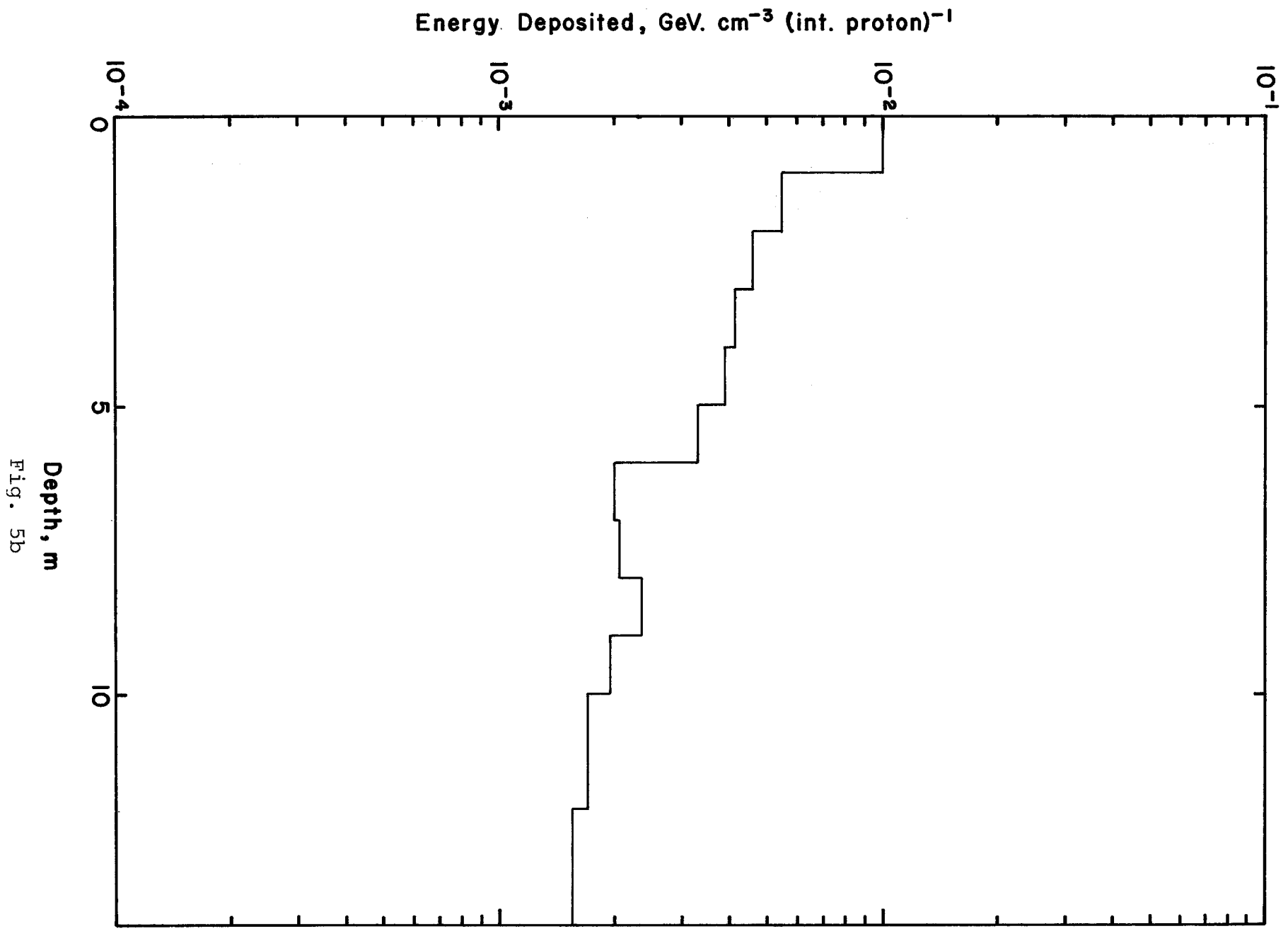
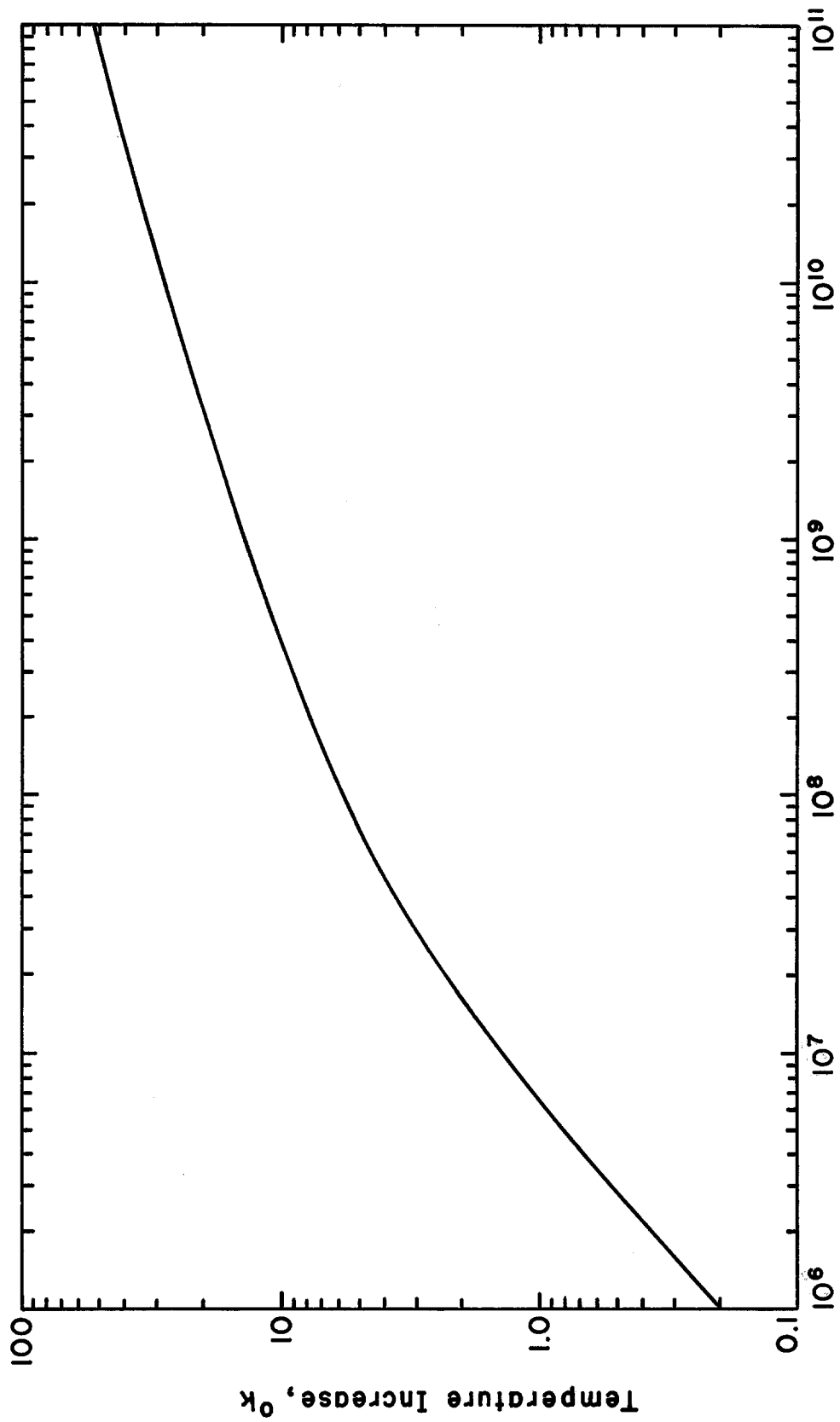


Fig. 5b



Energy Density, GeV. cm⁻³

Fig. 6